Biomaterials Science

ROYAL SOCIETY OF CHEMISTRY

PAPER

View Article Online
View Journal

Cite this: DOI: 10.1039/d4bm01038h

Photodynamic hemostatic silk fibroin film with photo-controllable modulation of macrophages for bacteria-infected wound healing

Xiaoxuan Tang, Wenpin Wu, Shuxuan Zhang, Chang He, Kewei Fan, Yulan Fan, Xuewa Yang, Jiaying Li,* Yumin Yang * and Jue Ling *

Massive hemorrhage and chronic wounds caused by bacterial infections after trauma are significant challenges in clinical practice. An ideal hemostatic wound dressing should simultaneously manage bleeding and prevent bacterial infections and also hold excellent biocompatibility and bioactivities to successfully modulate immune microenvironments to promote wound healing. In this study, a silk fibroin-based light-responsive film was demonstrated to possess effective capacity of light-induced non-compressible hemostasis on liver hemorrhage and tail bleeding *in vivo* by binding with blood platelets to promote the clotting cascade. The blood loss of the rats was significantly less after C-MASiF films were applied, which were 1223.33 ± 347.9 mg (liver trauma) and 363.33 ± 60.28 mg (tail trimming). Importantly, the films exhibited photo-controllable modulation activity on macrophages through repeated near-infrared irradiation to regulate the immune microenvironment to enhance photodynamic antibacterial therapy. Moreover, the light-responsive silk fibroin film effectively promoted *Staphylococcus aureus* infected burn wound healing *in vivo*. The quantity of residual bacteria in the wound sites of mice in the C-MASiF films group ($0.05 \pm 0.0047 \times 10^8$ CFU mL^{-1}) was considerably less than that in the control group ($3.18 \pm 0.75 \times 10^8$ CFU mL^{-1}), and the wound area in the C-MASiF group (78.03% ± 4.12%) was considerably smaller than that in the control group (60.33% ± 8.81%) after 14 days. Overall, this light-responsive silk fibroin film can provide a powerful strategy for wound healing of burns.

Received 6th August 2024,
Accepted 9th September 2024

DOI: 10.1039/d4bm01038h

rsc.li/biomaterials-science

Introduction

Massive hemorrhages are the main cause of death after severe trauma.[1–3] Additionally, serious trauma is usually highly susceptible to bacterial infection, which inhibits the normal wound healing process, leading to chronic wounds and severe abscesses.[4,5] Common wound dressings (including gauze, cotton, and polymer bandages) usually lack effective bioactivities and antibacterial activities. Thus, they cannot provide a damp and cell-favorable environment at the wound sites to promote cell growth nor do they prevent potential bacterial infections.[6,7] Moreover, traditional sutures are not only time-consuming but also require suitable instruments and skilled operators, making it difficult to immediately stop bleeding.[8,9] Therefore, an ideal hemostatic wound dressing should not only simultaneously manage bleeding and prevent bacterial infections but also hold good biocompatibility and bioactivities to successfully modulate immune microenvironments and promote wound healing.[10–12]

Silk fibroin (SF) as a natural protein is extracted from silkworms.[13,14] Due to its superior biocompatibility and adjustable mechanical strength, various SF-based biomaterials,

Key Laboratory of Neuroregeneration of Jiangsu and the Ministry of Education, Co-Innovation Center of Neuroregeneration, Medical School of Nantong University, Nantong University, Nantong, 226001, China

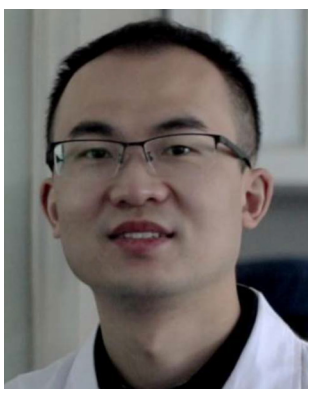

Jue Ling

Dr Jue Ling received his Ph.D. from Queen's University Belfast and currently works at the Key Laboratory of Neuroregeneration, Nantong University as a full professor of Biomedical Engineering. His research interests are in the preparation and applications of multifunctional materials in tissue engineering, particularly the preparation of light-responsive biomedical materials for tissue regeneration.

such as 2D films and hydrogels, have been developed for tissue engineering, wound healing, and nerve repair.[15–19] Moreover, SF has also been demonstrated to facilitate platelet adhesion on SF-based hemostatic materials to accelerate clotting cascades.[20–22] In particular, SF can facilitate cell adhesion and cell growth of various cell types (such as epithelium, endothelium, fibroblasts, and keratinocytes) in wound healing.[18,23,24] However, the lack of antibacterial activity and insufficient effect of regulating immune cells, such as macrophages, limit the further application of SF in bacteria-infected wound healing.[25–27]

Antibiotics are the most widespread and common means of clinical treatment for wound infections. However, antibiotic-resistant and multidrug-resistant bacteria have emerged due to their overuse.[28] Photodynamic antibacterial agents that can generate reactive oxygen species (ROS) to eliminate multidrug-resistant bacteria have been widely developed.[29–31] Chlorin e6 (Ce6), a simple porphyrin compound, can effectively generate ROS under light stimulation to kill bacteria with minimal invasion and has been demonstrated to successfully activate an immune response to enhance the photodynamic therapy.[32–35] However, Ce6 is easily cleared in the body, which limits the efficacy of photodynamic therapy (PDT) on treating bacterial infections.[36–38]

In this study, a Ce6-modified silk fibroin-based antibacterial hemostatic film (C-MASiF) was demonstrated to hold photo-controllable modulation activity on macrophages and successfully achieve fast light-induced hemostasis of non-compressible liver hemorrhage and tail bleeding in rats as desirable hemostatic agents. More importantly, the C-MASiF film exhibited high bactericidal efficiency under near-infrared (NIR) irradiation *in vivo*, controllably regulating macrophage activation through repeated NIR irradiation to regulate the immune microenvironment toward enhanced photodynamic antibacterial therapy, which effectively improved wound healing on burns with bacterial infection (Scheme 1).

Results and discussion

Morphology and coagulation effect of the silk fibroin-based film

The C-MASiF film was successfully fabricated according to our previous literature.[25] Fig. 1A shows that the C-MASiF film was transparent with a dark color because of the Ce6 immobilized on the protein chains of silk fibroin. The optical microscope images (Fig. 1B and C) show that the C-MASiF film fabricated

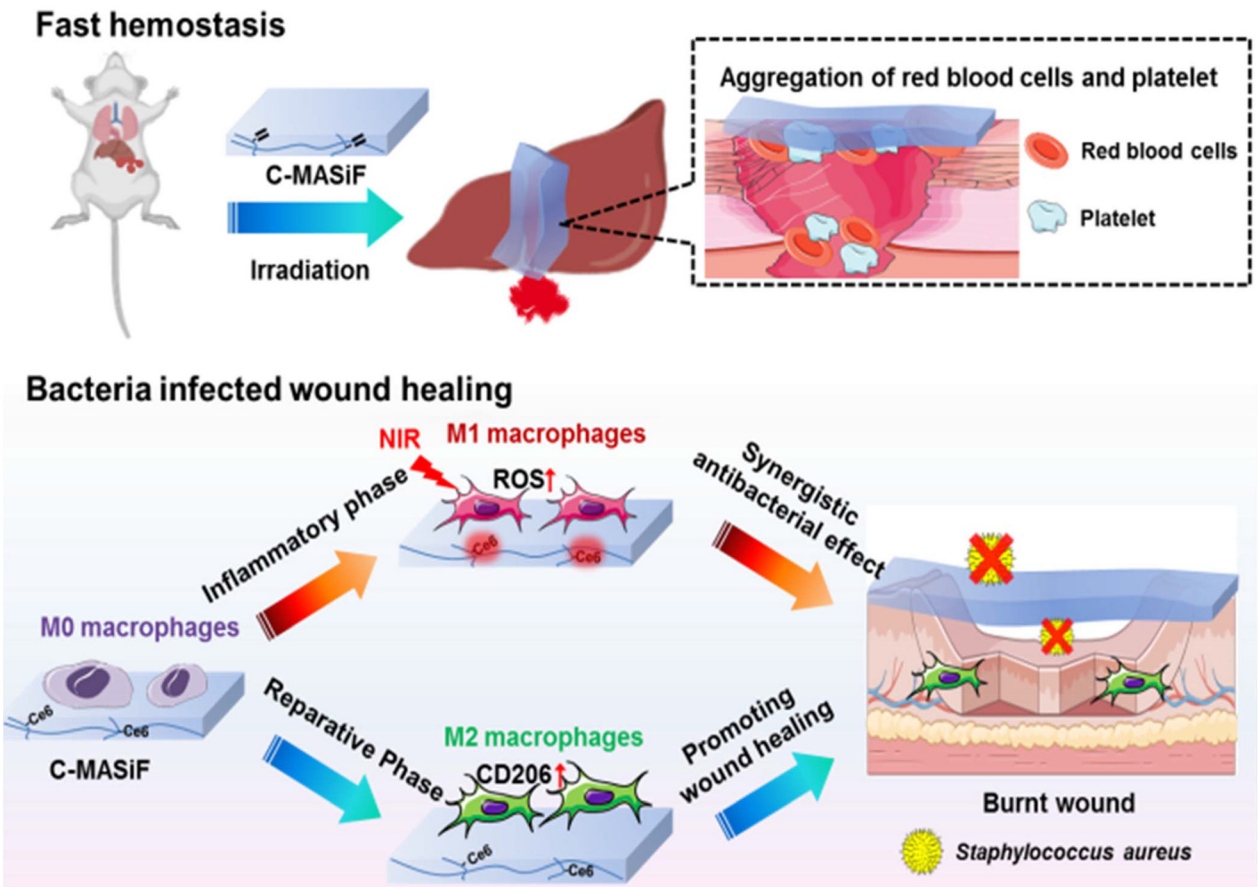

Scheme 1 A photodynamic hemostatic silk fibroin film with light-induced non-compressible hemostasis and photo-controllable macrophage polarization modulation activity was developed to regulate the immune microenvironment for promoting *Staphylococcus aureus* infected burn wound healing.

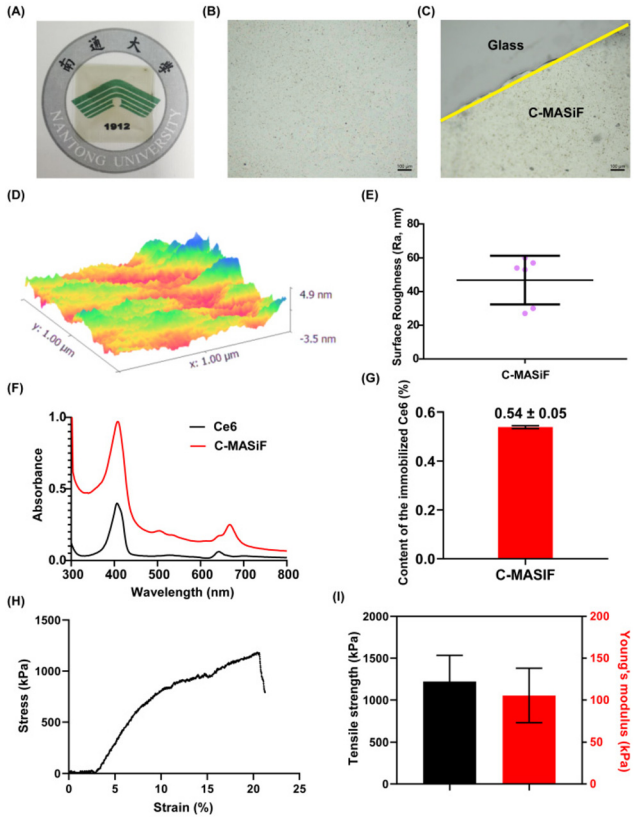

Fig. 1 Morphology and coagulation effect of C-MASiF. (A) Photographs of C-MASiF. (B and C) Microscopic images of C-MASiF, scale bar: 200 μm. (D) 3D structure of C-MASiF by atomic force microscopy. (E) Quantitative analysis of surface roughness (R_a), values represent means ± S.D. n = 6. (F) UV - vis spectra of Ce6 and C-MASiF (water as a solvent). (G) The content of the immobilized Ce6 on the C-MASiF, values represent means ± S.D. n = 3. (H) Stress–strain curve of C-MASiF. (I) Tensile strength or Young's modulus of C-MASiF, values represent means ± S.D. n = 5.

via casting and air drying methods had a uniformly dense morphology and smooth surface structure on the glass slide, which may facilitate the sealing of the bleeding sites by the C-MASiF film to achieve rapid hemostasis. Atomic force microscopy results indicated that the C-MASiF film had a surface roughness of 46.83 ± 14.44 nm (Fig. 1D and E).

Characteristic absorption peaks at 400 and at 640 nm appeared in the UV-vis spectrum of C-MASiF (Fig. 1F). To evaluate the content of immobilized Ce6 on the silk fibroin film, an absorbance of 0.5‰ solution of Ce6 conjugated methacrylated silk fibroin in hexafluoroisopropanol and 0.005‰ Ce6 hexafluoroisopropanol solution (as a standard sample) was recorded at 640 nm, respectively, to calculate the content of immobilized Ce6 on the silk fibroin film. As shown in Fig. 1G, the content of the immobilized Ce6 on the silk fibroin film was 0.54 ± 0.05% based on the absorbance at 640 nm. The mechanical properties of the film were evaluated using a tensile test. As shown in Fig. 1H and I, the tensile strength of the C-MASiF was 1221 ± 312.7 kPa, and the Young's modulus was 105.4 ± 32.62 kPa, which falls within the range of the Young's modulus value of human skin tissue (0.02 MPa–100 MPa),[39] suggesting that C-MASiF can adapt to dynamic movement.

Previously, we demonstrated that methacrylated silk fibroin-based materials can adhere to tissue by bonding between sulfhydryl groups and double bonds of the methacrylated silk fibroin under irradiation.[25] However, to achieve desirable hemostasis, the successful activation of a coagulation cascade usually relies on the effective aggregation of red blood cells (RBCs) and platelet adhesion, forming platelet thrombosis to stop the bleeding.[40] Moreover, previous studies have shown that silk fibroin can promote a clotting cascade by binding fibrinogen and platelets.[41] Therefore, the coagulation effect of C-MASiF films was further investigated by RBCs and platelet adhesion assays. RBCs and platelets were extracted from citrated whole blood of rabbit and respectively incubated with C-MASiF films at 37 °C for 1 h. As shown in the SEM images of Fig. 2A, the amounts of red blood cells and platelets adhered to the C-MASiF films were considerably higher than those on the glass slides. To further quantitatively analyze red blood cells and platelets adhered on C-MASiF films, a C-MASiF film or chitosan-coated glass (positive control) with red blood

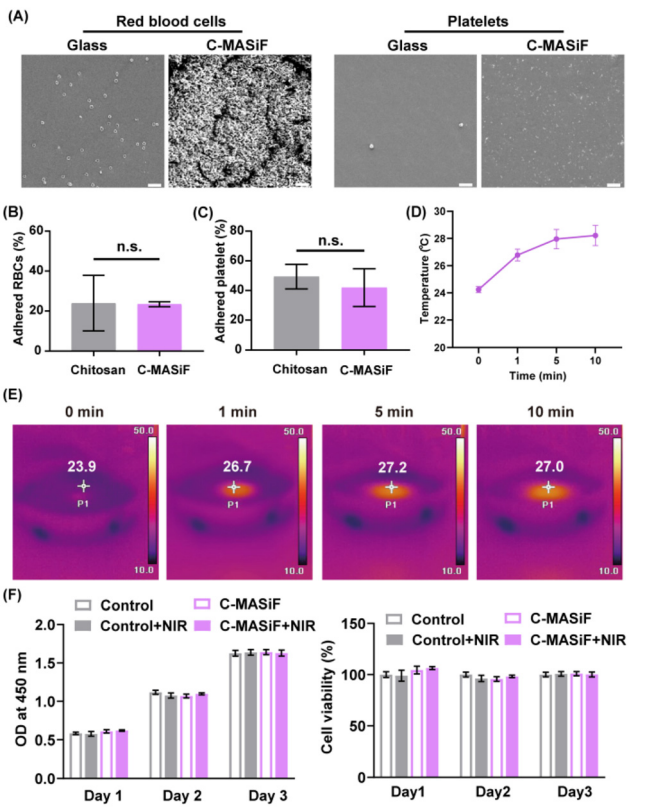

Fig. 2 (A–C) Coagulation effect of C-MASiF. SEM images of red blood cells (RBCs) and platelets adhered on C-MASiF (A), scale bar: 20 μm. Quantitative analysis of adhered RBCs (B) and PRP (C), values represent means ± S.D. n = 9. (D and E) Temperature variation by NIR irradiation, values represent means ± S.D. n = 3. (F) Viability of L929 fibroblasts cultured with C-MASiF for 3 days after NIR irradiation. Values represent means ± S.D. n = 9.

cells was immersed in deionized water at 37 °C for 1 h to destroy the adhered red blood cells to collect hemoglobin. The samples were soaked in 1% Triton X-100 solution to collect lactate dehydrogenase (LDH) from the adhered platelets and determined by the LDH kit. As shown in Fig. 2B and C, the adhesion ratio of RBCs and platelets in the C-MASiF films group was comparable to those in the chitosan groups with procoagulant properties, and there was no significant statistical difference between the two groups. These results indicated that the C-MASiF film could effectively induce the aggregation of red blood cells and platelet adhesion to activate the coagulation cascade to improve hemostasis after sealing the bleeding site, which might further form an effective mechanical barrier for wound closure.

To further evaluate the effect of NIR irradiation on the temperature of the C-MASiF film, the temperature of the film was recorded during 10 minutes of NIR irradiation. As shown in Fig. 2D and E, the temperature of the C-MASiF film only increases to 28.22 °C ± 0.74 °C even after 10 minutes of NIR irradiation, which was much lower than the normal body temperature (37 °C) and would not affect the healing would process. Fine cytocompatibility is essential for a well-designed biomaterial. To evaluate the effect photodynamic therapy on normal cells, L929 fibroblasts seeded on the C-MASiF film were NIR irradiation for 4 min and then further cultured for 3 days. The viability of cells was assessed with CCK-8 assay. As shown in Fig. 2F, no significant toxic effect on the cell proliferation of L929 fibroblasts was found after PDT treatment using the C-MASiF film.

Light-controllable macrophage activation by C-MASiF

It is known that the recruitment and activation of macrophages during the initial inflammatory phase considerably contribute in eliminating microorganisms and promoting the early stage of wound healing. However, excessive activation of macrophages can also result in pro-inflammatory responses and fibrosis.[42–45] Therefore, developing engineered biomedical materials with promising capacities on controllably modulating macrophage activation was desirable for preventing bacterial infections and promoting tissue regeneration. Thus, the photo-triggered modulation capacity of the film on macrophage activation was then investigated by incubating RAW264.7 cells with C-MASiF films, which was then stimulated with repeated NIR light (660 nm, 20 mW cm^{-2}) within 48 h. As shown in Fig. 3A and B, RAW264.7 cells incubated with C-MASiF films were successfully activated to M1 phenotype at 12 h after the first 4 min of NIR irradiation, and possessed significantly enhanced expression of inducible nitric oxide synthase (iNOS). This is due to the Ce6 moieties on the C-MASiF film, which generated ROS upon irradiation to promote M1 polarization of macrophages.[46] Interestingly, the iNOS expression of RAW264.7 cells in the C-MASiF film group was significantly reduced at 24 h after the first NIR irradiation with no significant statistical difference compared to the RAW264.7 cells in other groups, indicating that the RAW264.7 cells in the C-MASiF film group are gradually deactivated when

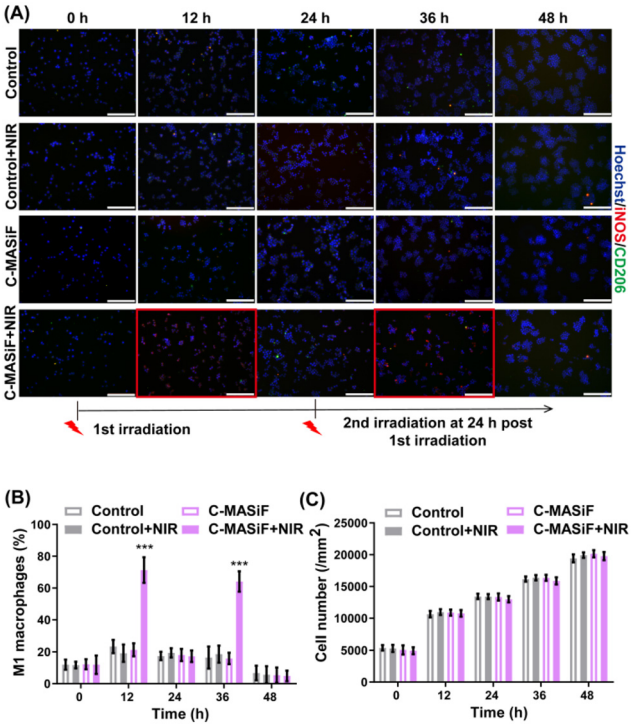

Fig. 3 Light-controllable macrophage activation by C-MASiF. (A) Fluorescence image of RAW264.7 cells during 48 h with repeated 4 min of NIR irradiation *in vitro* (iNOS (red, M1) and CD206 (green, M2)). Red squares indicate the effective activation of RAW264.7 cells at 12 h and 36 h post 1st irradiation, scale bar: 100 μm. Proportion of M1 macrophage (B) and cell proliferation of RAW264.7 cells (C), values represent means ± S.D. n = 9.

the NIR irradiation is turned off. Subsequently, upon repeated stimulation of 4 min NIR irradiation at 24 h after the first NIR irradiation, the deactivated RAW264.7 cells restored the high level of iNOS expression at 36 h after the first NIR irradiation and then slowly deactivated. Furthermore, neither RAW264.7 cells on the blank culture plate with NIR irradiation nor the RAW264.7 cells in the C-MASiF film without NIR irradiation was found to be effectively activated. These results demonstrate that the C-MASiF film can promisingly modulate the activation of macrophages in a controlled manner with repeated NIR irradiation. To eliminate the cytotoxic effect of low-dose ROS generated by the C-MASiF film upon 4 min of NIR irradiation on macrophages, the cell numbers of macrophages in all groups were counted. Fig. 3C shows that RAW264.7 cells in all groups proliferated normally during the experiments for 48 h without significant statistical difference, indicating that the C-MASiF film and certain low-doses of ROS had no cytotoxic effect on macrophages, which is essential for biomedical applications.

In vivo biocompatibility of the C-MASiF film

An ideal hemostatic wound dressing should hold good biocompatibility when applied *in vivo*.[47,48] To evaluate the *in vivo* biocompatibility of C-MASiF films, they were implanted under the dorsal skin of Sprague Dawley (SD) rats for 28 days.

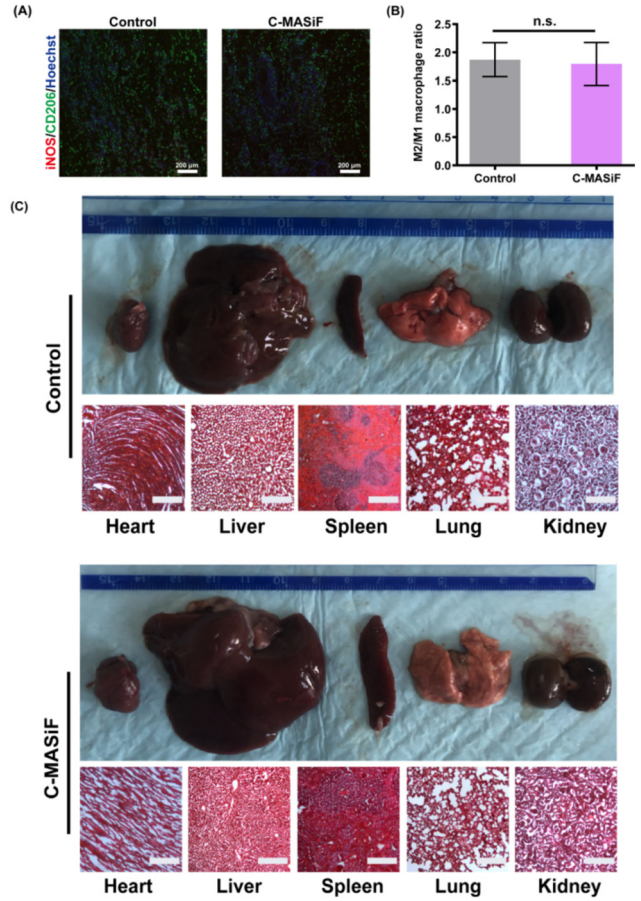

Fig. 4 *In vivo* biocompatibility of C-MASiF film. (A) Immunofluorescence staining of the tissue around the implantation site collected at day 14 (red: iNOS, M1; green: CD206, M2; blue: Hoechst 33342), scale bar: 200 μm. (B) Proportion of M2/M1 macrophage, values represent means ± S.D. n = 3. (C) Photographs of heart, liver, spleen, lung, and kidney tissues and images of H&E staining of each tissue at 28 days of implantation, scale bar: 200 μm.

Moreover, the skin tissue around the implantation site was collected at day 14 post implantation for further immunofluorescence staining analysis. As shown in Fig. 4A and B, the proportion of M2 type anti-inflammatory macrophages is significantly higher than M1 type pro-inflammatory macrophages (2.007 ± 0.3352). No severe inflammatory response was detected compared to normal tissues (1.962 ± 0.2954).

To evaluate whether the degradation products of the C-MASiF film have toxic side effects on the body, such as thrombosis and other damage to main organs, C-MASiF films were implanted subcutaneously in SD rats. The rats were then perfused at day 28 post-implantation. Heart, liver, spleen, lung, and kidney tissues were collected for frozen sectioning and histologic analyses using hematoxylin–eosin staining (H&E staining). As shown in Fig. 4C, the implantation of the C-MASiF film had no significant side effect on the shape and size of the main organs of rats compared to those of healthy rats. An additional H&E staining assay showed that there was no overt detrimental effect on the various internal organs of rats in the C-MASiF film group, indicating no significant side effects on the circulatory, respiratory, digestive, or metabolic systems. These results suggested that the C-MASiF film exhibited excellent *in vivo* biocompatibility for *in vivo* applications.

Photodynamic antibacterial therapeutic effect of the C-MASiF film

Besides massive hemorrhages, extensive wound exposure is usually at high risk of bacterial infection, leading to chronic wounds and even death. Therefore, antibacterial properties are critical in developing multifunctional hemostatic dressings.[49–51] Thus, the photodynamic antibacterial effect of C-MASiF films on *Staphylococcus aureus* (*S. aureus*) was investigated. As shown in Fig. 5A and B, the proportion of dead bacteria on the C-MASiF films was 88% ± 3.162% after 10 min of NIR irradiation (20 mW cm^{-2}). This was due to the effective production of ROS by the Ce6 moiety, which was significantly higher than that of the control group (3.6% ± 2.608%). C-MASiF films without NIR irradiation exhibited no antibacterial activity (3.6% ± 2.966%). These results illustrated the poor antibacterial property of NIR light or C-MASiF film alone, but effective photodynamic antibacterial performance of the C-MASiF film upon irradiation.

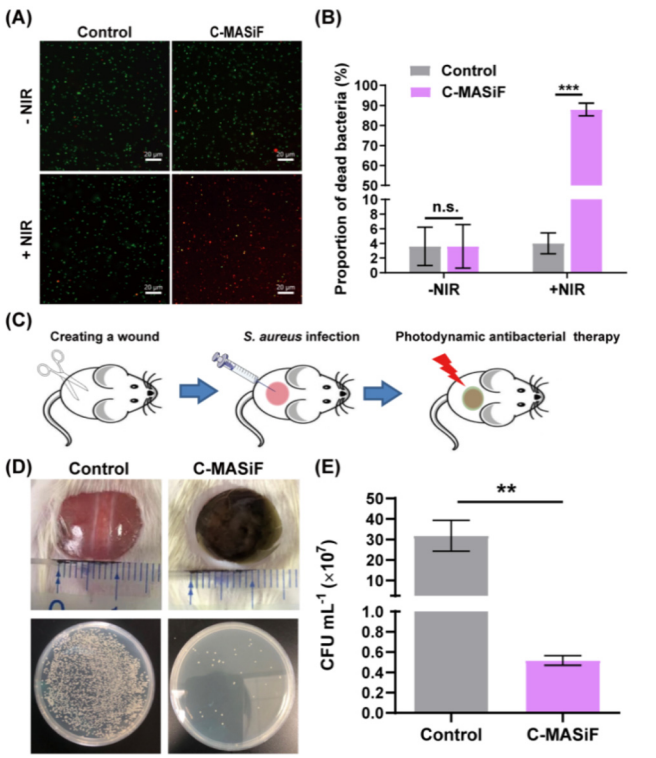

Fig. 5 Photodynamic antibacterial therapeutic effect of C-MASiF film against *S. aureus*. (A) Live/dead bacteria staining (green: live bacteria; red: dead bacteria), scale bar: 20 μm. (B) Proportion of dead bacteria, n = 5. (C) Schematic depiction of *in vivo* photodynamic antibacterial therapy. (D) Photographs of *S. aureus* infected wound of rats treated with C-MASiF film and residual bacteria from wound sites at day 3. (E) Quantitative analysis of antibacterial efficiency *in vivo*, n = 3, values represent means ± S.D.

To further validate the *in vivo* photodynamic antibacterial activity of C-MASiF films, the infected wound mouse model was established by creating a round wound (diameter: 10 mm) on the back of BALB/c mice that was infected with *S. aureus*. Then, infected wounds were treated with C-MASiF films or saline (control group), and respectively irradiated by NIR light (20 mW cm^{-2}) for 10 min (Fig. 5C). The infected wound mouse models were then individually housed in cages. To evaluate the residual bacteria remaining at the wound site after treatment, skin tissues from each group were collected on the third day post-treatment, and microorganisms in the tissues were extracted using sterile phosphate-buffered saline (PBS). As shown in Fig. 5D and E, the number of residual bacteria in the wound sites of mice in the C-MASiF films group ($0.05 \pm 0.0047 \times 10^8$ CFU mL^{-1}) was significantly less than that in the control group ($3.18 \pm 0.7529 \times 10^8$ CFU mL^{-1}). These results indicated that the C-MASiF film possessed promising *in vivo* photodynamic antibacterial activities to prevent bacterial infections after trauma.

In vivo hemostatic effect of C-MASiF film

To further investigate the *in vivo* hemostatic effect of the C-MASiF film for potential applications in various clinical scenarios, the rat liver trauma model and tail trimming model were established by cutting a gap of 2 ± 0.5 cm in the liver or cutting off the proximal 1/4 position of the tail. Then, C-MASiF films containing Irgacure 2959 were applied on the gap in the liver or injured tail with UV irradiation (365 nm, 50 mW cm^{-2}) for 2 min (Fig. 6A and C). The blood loss of the rats with liver trauma and tail trimming in the control group (without any treatment) were 2036.67 ± 297.0 mg and 683.33 ± 189.0 mg, respectively. Moreover, the blood loss in the C-MASiF group was significantly less after the C-MASiF films were applied, which were 1223.33 ± 347.9 mg (liver trauma) and 363.33 ± 60.28 mg (tail trimming), respectively (Fig. 6B and D). These results indicated that the C-MASiF film possessed a strong capacity for light-induced non-compressible hemostasis *in vivo* because of the rapid photoreaction between the C-MASiF film and tissue, and the excellent capacities of the C-MASiF film on facilitating pro-coagulation cascades by aggregating red blood cells and platelet adhesion.[25]

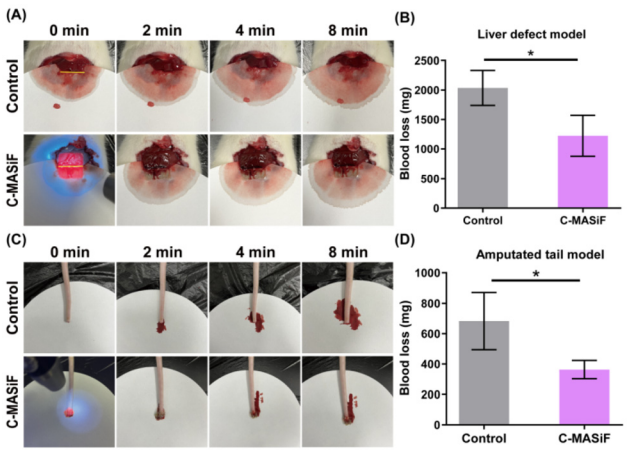

Fig. 6 Liver and tail hemostasis *in vivo*. (A) Photographs of liver hemostasis using C-MASiF film. (B) Blood loss of liver hemostasis, n = 3. (C) Photographs tail hemostasis using C-MASiF film. (D) Blood loss of tail hemostasis, n = 3. Values represent means ± S.D.

Therapeutic effect of C-MASiF films on promoting infected burn wound healing

Burn wounds are a complex and severe form of skin trauma, with large burn areas, tissue necrosis, and susceptibility to infection, which are extremely common in daily life.[52] Silk fibroin-based biomaterials have been reported to promote skin regeneration by recruiting macrophages, fibroblasts, and other cells to the wound site. However, the lack of antibacterial activity limits the application of silk fibroin-based biomaterials in bacteria-infected burn wounds.[23,53] Therefore, to evaluate the therapeutic effect of C-MASiF films on promoting the healing of bacteria-infected burn wounds, a common infected burn model on the back of mice was established by following a procedure in the literature[54,55] (Fig. 7A). Infected burn wounds were treated with C-MASiF films or saline (control group), and respectively irradiated by NIR light (20 mW cm^{-2}) for 10 min. As shown in Fig. 7B, the *S. aureus* infection at the wound site of mice in the C-MASiF group was significantly relieved when compared with that of the control group. Furthermore, no abscess was observed due to the promising photodynamic antibacterial activity of the C-MASiF film and enhanced initial immune response. Conversely, mice in the control group showed severe abscesses in the burn wounds. The wound area in the C-MASiF group (78.03% ± 4.12%) was significantly smaller than that in the control group (60.33% ± 8.81%) after 14 days (Fig. 7C). Tissues from the wound sites in each group were collected at day 14, and further analyzed by hematoxylin–eosin (H&E) staining. As shown in Fig. 7D, histological examination indicated that the wounds in the C-MASiF group exhibited a connective epithelium layer with high regularity and more blood vessels and hair follicles compared to the control group, contributing function to the healed skin.[56] Conversely, there was more inflammatory cell infiltration in the control group. In the later stage of wound healing, M2 polarization of macrophages can significantly facilitate tissue regeneration.[57] Therefore, the infiltration and polarization of macrophages in the wound sites was analyzed by immunofluorescence staining the tissue for iNOS as a marker of M1 immunostimulatory phenotype and CD206 as a marker of M2 immunosuppressive phenotype at day 14. As shown in Fig. 7E, corroborating with histological examination, a significantly larger amount of M1 pro-inflammatory macrophages was found in the wound sites in the control group due to the bacterial infection. However, significantly reduced pro-inflammatory macrophage infiltration and a higher proportion of M2 macrophages to M1 macrophages were found in the C-MASiF group due to the photodynamic antibacterial and inflammatory regulatory effects of the C-MASiF film.[57,58] More importantly, the M2 macrophages mainly recruited surrounding blood vessels

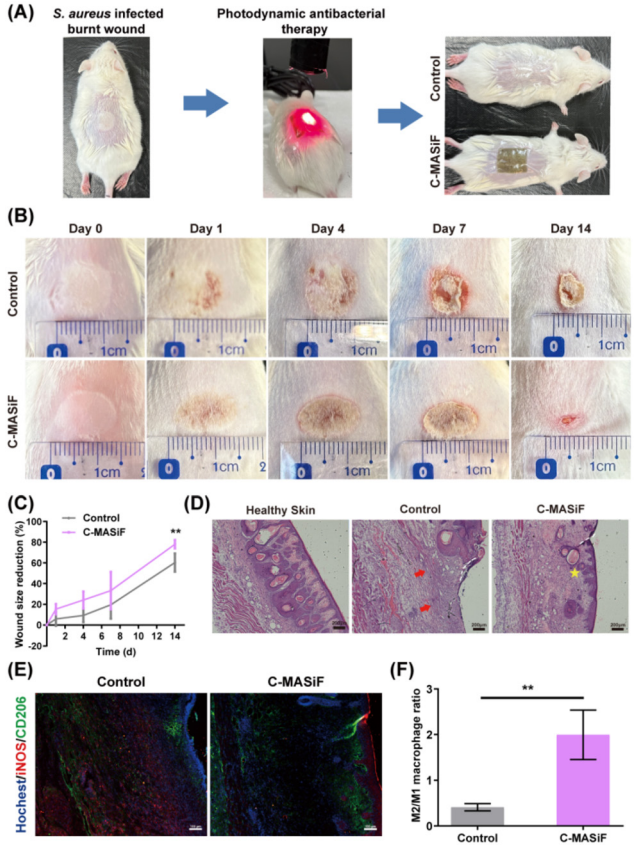

Fig. 7 C-MASiF films on promoting infected burnt wound healing. (A) Schematic illustration of *in vivo* experiments. (B) Representative photographs of wound sites during 14 days post treatment. (C) Quantitative analysis of the wound area, $n = 5$. (D) H&E staining of regenerated tissue on day 14 (white dashed line: the junction between the wound and normal tissue; red arrow: aggregation of inflammatory cells; yellow pentagram: blood vessel/hair follicle), scale bar: 200 μm. (E) Macrophage distribution in wound tissue visualized by immunofluorescence staining (nucleus (blue), iNOS (M1, red), and CD206 (M2, green)), scale bar: 100 μm. (F) Ratio of M2/M1 macrophages, $n = 3$. Values represent means ± S.D.

and hair follicles in the regenerated skin tissue in the C-MASiF group, which could promote the proliferation and differentiation of vascular endothelial cells by secreting vascular endothelial growth factors to stimulate blood vessels and hair follicle regeneration (Fig. 7F),[59,60] which was consistent with the results of H&E staining. These results revealed that C-MASiF could positively promote *S. aureus*-infected burn wound recovery by its effective photodynamic antibacterial property and inflammatory regulatory capacity.

Experimental

Fabrication of C-MASiF

C-MASiF was successfully fabricated according to the previously reported method.[25] Briefly, 5 mL Ce6 (Frontier Scientific, USA) solution (0.1%, w/v) containing 30 mg 1-(3-(dimethylamino) propyl)-3-ethylcarbodiimide hydrochloride (EDC) (TCI, China) and 30 mg *N*-hydroxysuccinimide (NHS) (Sigma-Aldrich, USA) was introduced into 50 mL methacrylated silk fibroin solution (1%, w/v). The mixture was stirred overnight at 4 °C in the dark, subsequently dialyzed at 4 °C for 2 days, and then lyophilized. The freeze-dried powder was dissolved in deionized water to prepare a 15% (w/v) solution of Ce6-conjugated methacrylated silk fibroin, then 400 μL solution was added dropwise onto a square glass slide (22 mm × 22 mm), and air dried at 4 °C to form a C-MASiF film. Then, C-MASiF was treated with anhydrous ethanol to obtain the β-folding of silk fibroin (Yonghua Chemical Technology Co., Ltd, China). The morphology of the C-MASiF film was observed by ZEISS-AX10 (Carl Zeiss AG, Germany).

Atomic force microscopy (AFM)

The morphology and roughness of the C-MASiF film were further investigated using atomic force microscopy (FM-Nanoview 6800, Flyman Precision Instrument Co., Ltd, China). The C-MASiF film was fixed on the platform and scanned using tap mode. The area of the test was 1.0 × 1.0 μm and the amplitude of the vibration source was 0.1 V.

Content of immobilized Ce6 on the silk fibroin film

To evaluate the content of immobilized Ce6 on the silk fibroin film, the absorbance of 0.5‰ solution of Ce6-conjugated methacrylated silk fibroin in hexafluoroisopropanol and 0.005‰ Ce6 hexafluoroisopropanol solution (as a standard sample) was recorded at 640 nm respectively to calculate the content of immobilized Ce6 on the silk fibroin film by UV-vis spectroscopy (UV-2450, Shimadzu, Japan).

Mechanical test

Tensile-strength measurements were performed using an electronic universal testing machine (UTM, TFW-58, China). Samples with 17 mm width and 0.1 mm thickness were tested at a displacement rate of 2 mm min^{-1} at room temperature.

Red blood cells adhesion assay

RBCs were extracted from citrated whole blood obtained from New Zealand rabbits by centrifugation (400*g*, 10 min). 100 μL of red blood cell suspension was incubated with glass sides, C-MASiF films and chitosan films for 1 h at 37 °C. Then, the glass sides and films were washed with PBS for three times. Adherent red blood cells on samples were characterized by scanning electron microscope (S-3400N II, Hitachi, Japan). Then, 4 mL of deionized water was added and incubated at 37 °C for 1 h to destroy the adhered RBCs and release hemoglobin. The 100 μL supernatant was transferred to a 96-well microplate, and then its OD value at 540 nm was measured by an ElX-800 microelisa reader.

$$\text{Adhered RBCs } (\%) = OD_{sample}/OD_{control} \times 100\%$$

OD_{sample}, the OD540 nm value treated with samples; $OD_{control}$, the OD540 nm value without treatment.

Platelet adhesion assay

Platelet-rich plasma (PRP) was extracted from citrated whole blood obtained from New Zealand rabbits by centrifugation (400*g*, 10 min). 100 μL of PRP was incubated with glass sides, C-MASiF films and chitosan films for 1 h at 37 °C. Then, the glass sides and films were washed with PBS for three times. Adherent platelets were characterized by scanning electron microscope (S-3400N II, Hitachi, Japan). Lactate dehydrogenase was further extracted from adherent platelets on the samples using 1% Triton X-100 solution, and then determined by LDH kit (Shanghai Biyuntian Biotechnology Co., Ltd, China) according to instructions.

$$\text{Adhered platelets } (\%) = \text{OD}_{\text{sample}}/\text{OD}_{\text{control}} \times 100\%$$

$\text{OD}_{\text{sample}}$, the OD490 nm value treated with samples; $\text{OD}_{\text{control}}$, the OD490 nm value without treatment.

Temperature variation by NIR irradiation

The C-MASiF was exposed continuously under a 660 nm laser for 10 minutes, and the temperature of the C-MASiF film was recorded using an infrared thermal imager (HIKMICRO, China).

Cytotoxicity

The cytotoxicity of the hydrogels was assessed by the cell counting kit-8 (CCK-8) (Beyotime Biotechnology, China). The mouse fibroblast (L929) cells (Cell Bank of the Chinese Academy of Sciences, China) were seeded on C-MASiF in the 24-well plate with a density of 30 000 cells per mL per well, and irradiated under NIR laser (20 mW cm^{-2}) for 4 min, then incubated for 24, 48 and 72 h. 100 μL CCK-8 reagent was added to each well and incubated for 4 h at 37 °C. Then, the absorbance of each well was measured at 450 nm by an ElX-800 microelisa reader. The relative cell viability was calculated as follows:

$$\text{Cell viability } (\%) = \text{Abs}_{\text{experiment}}/\text{Abs}_{\text{control}} \times 100\%.$$

Light-controllable macrophage activation

RAW264.7 cells (1×10^4 cells per well) were seeded in 24-well plates, and C-MASiF films were then incubated with RAW264.7 cells and followed by NIR irradiation (660 nm, 20 mW cm^{-2}) for 4 min. At 24 h after the first NIR irradiation, C-MASiF films incubated with RAW264.7 cells were irradiated again with NIR light (660 nm, 20 mW cm^{-2}) for 4 min and cells were continuously incubated for another 24 h. During the experiment, RAW264.7 cells were immunofluorescence stained at 0, 12, 24, 36, 48 h with the anti-iNOS rabbit monoclonal antibody (1 : 400, 18985-1-AP, Proteintech, USA), anti-CD206 mouse monoclonal antibody (1 : 400, 60143-1-Ig, Proteintech, USA), goat anti-mouse Alexa Fluor 488-conjugated preadsorbed antibody (1 : 400, ab150113, Abcam, USA), goat anti-rabbit Alexa Fluor Cy3-conjugated preadsorbed antibody (1 : 400, ab97075, Abcam, USA) and Hoechst 33342 (1 : 20, Thermo Fisher Scientific, USA), and then imaged using a fluorescence microscope (DM2500, Leica, Germany).

Photodynamic killing of *S. aureus in vitro*

100 μL of *S. aureus* (~10^8 CFU mL^{-1}) obtained from China Microbial Culture Collection were inoculated on the surface of the blank plate or C-MASiF, incubated at 37 °C for 20 min, and then subsequently irradiated with or without a NIR laser (660 nm, 20 mW cm^{-2}) for 10 min, respectively. Then, PBS was used to resuspend the *S. aureus*, and the *S. aureus* solution was then stained with Calcein-AM and PI (CA1630-500T, solarbio, China) for 20 min in the dark. The stained bacterial suspension was spread onto a 18 mm square glass slide and imaged using a fluorescence microscope (Axioscope 5, Zeiss, Germany).

Photodynamic killing of *S. aureus in vivo*

All animal procedures were performed in accordance with the Guidelines for Care and Use of Laboratory Animals of Nantong University, and approved by the Animal Ethics Committee of Nantong University.

The *Staphylococcus aureus* infection model was established by cutting the round wound (10 mm diameter) on the back of 6-week-old male ICR mice, and 50 μL clinically isolated *S. aureus* suspension (1×10^7 CFU mL^{-1}) was applied to the wound sites. These mice were then randomly divided into two groups. C-MASiF and saline (control group) were used to treat the infected wounds respectively, which then underwent NIR treatment (660 nm, 20 mW cm^{-2}) for 10 min. The mice were subsequently housed in cages individually for 3 days. Tissue at the wound sites of the mice was collected, and microorganisms were extracted from the tissue using sterile PBS. Microorganism colonies on solid LB agar plates were counted after incubating the diluted microorganism suspension at 37 °C for 24 h. The results were expressed as the bacterial kill rate:

$$\text{kill}\% = (C_0 - C)/C_0 \times 100\%$$

where C is the CFU of the experimental group, and C_0 is the CFU of the control group.

In vivo degradation and histologic analysis of C-MASiF

C-MASiF samples were weighed and implanted under the dorsal skin of SD rats. Then, at days 4, 7, 14, and 28, the rats were sacrificed and the samples were collected for further histologic analysis. The results of the degradation rate were determined as follows:

$$\text{Degradation rate} = (W_0 - W_t)/W_0 \times 100\%$$

where W_t is the weight of C-MASiF after implantation, and W_0 is the initial weight.

Immunofluorescence staining of the tissue around the sample implantation site at day 14 was performed to evaluate the expression of iNOS (1 : 400, 18985-1-AP, Proteintech, USA) and CD206 (1 : 400, 60143-1-Ig, Proteintech, USA). The stained tissue was then imaged using a fluorescence microscope (DM2500, Leica, Germany) with normal tissue as the control.

At day 28, the rats were perfused with a 4% paraformaldehyde solution, and heart, liver, spleen, lung, and kidney were collected. Tissue was frozen-sectioned for hematoxylin and eosin (H&E) staining. Healthy SD rats were used as the control.

Hemostatic test *in vivo*

After shaving and disinfecting the abdomen of anesthetized SD rats, their abdominal cavities were opened to expose the livers. The liver was placed on the surface of pre-weighed gauze and filter paper, and a gap of 2 ± 0.5 cm was cut. Then, the gap was covered using the C-MASiF film with a photo-initiator (Irgacure 2959). The hemostatic film was allowed to adhere to the liver upon UV light (365 nm, 50 mW cm^{-2}) for 2 min. The amount of bleeding on filter paper was measured.

After fixing the anesthetized SD rats, their tails were wiped with alcohol for disinfection. The proximal 1/4 position of the tail was cut, which was immediately covered using the C-MASiF film with a photo-initiator (Irgacure 2959). The hemostatic film was allowed to adhere to the liver upon UV light (365 nm, 50 mW cm^{-2}) for 2 min. The amount of bleeding on the filter paper was measured.

Infected burn wound repair

The back hair of the anesthetized mice was shaved. Then, an iron nail with a diameter of 10 mm was heated in boiling water and transferred immediately to the back of the mouse, and contact was maintained for 30 s. After cooling for 10 min, 50 μL of *S. aureus* (1×10^7 CFU mL^{-1}) was injected subcutaneously at the scald site. Burn wounds were covered with C-MASiF films or washed with saline, respectively, followed by NIR (660 nm, 20 mW cm^{-2}) treatment for 10 min. After surgery, each mouse was raised in a single cage to ensure free feeding. Photographs of the wounds were taken on days 0, 1, 4, 7, and 14, and the wound area was measured using Image J software. At day 14 post-treatment, wound tissues were collected. Subsequently, frozen sections were obtained and stained with H&E or immunofluorescence (iNOS (1 : 400, 18985-1-AP, Proteintech, USA) and CD206 (1 : 400, 60143-1-Ig, Proteintech, USA)). Images were examined using a fluorescence microscope (DM2500, Leica, Germany).

Data analysis

All experimental results were analyzed using Graphpad Prism 8.0 and Image J software. Results are expressed as the mean ± standard deviation (SD), and differences between the two groups were analyzed by a two-tailed, unpaired Student's *t* test. The $p < 0.05$ was considered significant ($^*p < 0.05$, $^{**}p < 0.01$, and $^{***}p < 0.001$).

Conclusions

In summary, a multifunctional silk fibroin-based hemostatic wound dressing with photo-antibacterial properties was developed for non-compressible hemostasis and the promotion of bacteria-infected wound healing. The C-MASiF film had a surface roughness of 46.83 ± 14.44 nm, the tensile strength of the C-MASiF was 1221 ± 312.7 kPa, and the Young's modulus was 105.4 ± 32.62 kPa. This antibacterial hemostatic film had excellent procoagulant properties and *in vivo* biocompatibility to achieve rapid hemostasis on non-compressible liver and tail bleeding in rats. The blood loss of the rats was significantly less after the C-MASiF films were applied, which were 1223.33 ± 347.9 mg (liver trauma) and 363.33 ± 60.28 mg (tail trimming). Importantly, the film controllably regulated macrophage activation through repeated NIR irradiation to modulate the immune microenvironment to enhance photodynamic antibacterial therapy for accelerating the repair of *S. aureus* infected burn wounds. The number of residual bacteria in the wound sites of mice in the C-MASiF films group ($0.05 \pm 0.0047 \times 10^8$ CFU mL^{-1}) was significantly less than that in the control group ($3.18 \pm 0.75 \times 10^8$ CFU mL^{-1}), and the wound area in the C-MASiF group (78.03% ± 4.12%) was significantly smaller than that in the control group (60.33% ± 8.81%) after 14 days. Therefore, we believe that this silk fibroin-based hemostatic film has great potential for applications in hemostasis, antiinfection and tissue repair.

There are some limitations in this study. The use of UV and UV initiators to achieve tissue adhesion is not desirable in clinic use. Thus, in future studies, to minimize the toxicity of UV light, up-conversion nanoparticles can be combined with current thin films to achieve effective tissue adhesion with visible or NIR light.[61] In terms of eliminating UV initiators, novel photosensitive functional groups, such as *o*-nitrobenzene, can also be introduced into silk fibroin chains to achieve effective tissue adhesion under blue light without any photoinitiator.[62]

Author contributions

Xiaoxuan Tang: methodology, investigation, formal analysis, writing – original draft. Wenpin Wu: formal analysis, investigation, writing – original draft. Shuxuan Zhang: methodology, writing – original draft. Chang He: methodology, investigation. Kewei Fan: methodology, investigation. Yulan Fan: investigation, formal analysis. Xuewa Yang: investigation, formal analysis. Jiaying Li: conceptualization, resources, project administration, funding acquisition, writing. Yumin Yang: supervision, investigation, resources, project administration, funding acquisition, writing. Jue Ling: supervision, conceptualization, methodology, formal analysis, visualization, project administration, writing.

Data availability

All relevant data are within the paper.

Conflicts of interest

There are no conflicts to declare.

Acknowledgements

This research was financially supported by the National Natural Science Foundation of China (Project No. 32230057, 32471412), Natural Science Foundation of Jiangsu Province (Project No. BE2022766), Natural Science Foundation of the Higher Education Institutions of Jiangsu Province (22KJA310003), and the Jiangsu Provincial Key Medical Center and Nantong University (2023JY028).

References

1 X. Yang, W. Liu, N. Li, M. Wang, B. Liang, I. Ullah, A. L. Neve, Y. Feng, H. Chen and C. Shi, *Biomater. Sci.*, 2017, **5**, 2357–2368.
2 W. Wang, X. Liu, Y. Wang, D. Zhou and L. Chen, *Biomater. Sci.*, 2024, **12**, 4065–4082.
3 X. Zhao, Y. Huang, Z. Li, J. Chen, J. Luo, L. Bai, H. Huang, E. Cao, Z. Yin, Y. Han and B. Guo, *Adv. Mater.*, 2024, **36**, 202308701.
4 A. Joorabloo and T. Liu, *Exploration*, 2024, **4**, 20230066.
5 S. Lin, H. Chen, R. Wang, T. Jiang, R. Wang and F. Yu, *Biomater. Sci.*, 2023, **11**, 4874–4889.
6 S. O. Blacklow, J. Li, B. R. Freedman, M. Zeidi, C. Chen and D. J. Mooney, *Sci. Adv.*, 2019, **5**, eaaw3963.
7 J. Ma and C. Wu, *Exploration*, 2022, **2**, 20210083.
8 P. Sarkar, A. S. Pugazhendhi, M. Coathup and K. Mukhopadhyay, *Biomater. Sci.*, 2024, **12**, 4155–4169.
9 Q. Lei, D. He, L. Ding, F. Kong, P. He, J. Huang, J. Guo, C. J. Brinker, G. Luo, W. Zhu and Y. Yu, *Adv. Funct. Mater.*, 2022, **32**, 2113269.
10 B. Guo, R. Dong, Y. Bang and M. Li, *Nat. Rev. Chem.*, 2021, **5**, 773–791.
11 M. Li, G. Pan, Y. Yang and B. Guo, *Nano Today*, 2023, **48**, 101720.
12 S. Pourshahrestani, E. Zeimaran and M. B. Fauzi, *Biomater. Sci.*, 2024, **12**, 3293–3320.
13 C. Vepari and D. L. Kaplan, *Prog. Polym. Sci.*, 2007, **32**, 991–1007.
14 S. Patil and N. Singh, *Biomater. Sci.*, 2019, **7**, 4687–4697.
15 J. Li, Z. Ding, X. Zheng, G. Lu, Q. Lu and D. L. Kaplan, *J. Mater. Chem. B*, 2021, **9**, 7771–7781.
16 A. Bigham, A. O. M. Salehi, M. Rafienia, M. R. Salamat, S. Rahmati, M. G. Raucci and L. Ambrosio, *Mater. Sci. Eng., C*, 2021, **127**, 112242.
17 X. Tang, X. Gu, T. Huang, X. Chen, Z. Zhou, Y. Yang and J. Ling, *ACS Macro Lett.*, 2021, **10**, 1501–1509.
18 X. Wan, Y. Zhao, Z. Li and L. Li, *Exploration*, 2022, **2**, 20210029.
19 D. N. Rockwood, R. C. Preda, T. Yucel, X. Wang, M. L. Lovett and D. L. Kaplan, *Nat. Protoc.*, 2011, **6**, 1612–1631.
20 C. Lei, H. Zhu, J. Li, X. Feng and J. Chen, *J. Biomater. Sci., Polym. Ed.*, 2016, **27**, 403–418.
21 D. Chouhan and B. B. Mandal, *Acta Biomater.*, 2020, **103**, 24–51.
22 M. Santin, A. Motta, G. Freddi and M. Cannas, *J. Biomed. Mater. Res.*, 1999, **46**, 382–389.
23 Z. Ekemen, Z. Ahmad, E. Stride, D. Kaplan and M. Edirisinghe, *Biomacromolecules*, 2013, **14**, 1412–1422.
24 Y. R. Park, M. T. Sultan, H. J. Park, J. M. Lee, H. W. Ju, O. J. Lee, D. J. Lee, D. L. Kaplan and C. H. Park, *Acta Biomater.*, 2018, **67**, 183–195.
25 T. Huang, Z. Zhou, Q. Li, X. Tang, X. Chen, Y. Ge and J. Ling, *Front. Bioeng. Biotechnol.*, 2022, **9**, 820434.
26 B. Cheng, Y. Yan, J. Qi, L. Deng, Z.-W. Shao, K.-Q. Zhang, B. Li, Z. Sun and X. Li, *ACS Appl. Mater. Interfaces*, 2018, **10**, 12474–12484.
27 A. Baba, K. Kitayama, T. Asakura, H. Sezutsu, A. Tanimoto and T. Kanekura, *J. Invest. Dermatol.*, 2015, **135**, S31.
28 S. Patil and N. Singh, *Biomater. Sci.*, 2019, **7**, 4687–4697.
29 D. Cao, H. He, W. Li, J. Yan and L. Yin, *Biomater. Sci.*, 2021, **9**, 4054–4065.
30 P. Lu, X. Zhang, F. Li, K.-F. Xu, Y.-H. Li, X. Liu, J. Yang, B. Zhu and F.-G. Wu, *Pharmaceuticals*, 2022, **15**, 1556.
31 Z. Chen, J. Yao, J. Zhao and S. Wang, *Int. J. Biol. Macromol.*, 2023, **225**, 1235–1245.
32 D. Mao, F. Hu, Z. Yi, K. Kenry, S. Xu, S. Yan, Z. Luo, W. Wu, Z. Wang, D. Kong, X. Liu and B. Liu, *Sci. Adv.*, 2020, **6**, eabb2712.
33 L. Sun, Q. Li, M. Hou, Y. Gao, R. Yang, L. Zhang, Z. Xu, Y. Kang and P. Xue, *Biomater. Sci.*, 2018, **6**, 2881–2895.
34 T. Zhou, R. Hu, L. Wang, Y. Qiu, G. Zhang, Q. Deng, H. Zhang, P. Yin, B. Situ, C. Zhan, A. Qin and B. Z. Tang, *Angew. Chem., Int. Ed.*, 2020, **59**, 9952–9956.
35 X. Tang, X. Chen, S. Zhang, X. Gu, R. Wu, T. Huang, Z. Zhou, C. Sun, J. Ling, M. Liu and Y. Yang, *Adv. Funct. Mater.*, 2021, **31**, 2101320.
36 B.-P. Jiang, L. Zhang, X.-L. Guo, X.-C. Shen, Y. Wang, Y. Zhu and H. Liang, *Small*, 2017, **13**, 1602496.
37 S. Theivendran, S. Lazarev and C. Yu, *Exploration*, 2023, **3**, 20220086.
38 X. Wang, M. Li, Y. Hou, Y. Li, X. Yao, C. Xue, Y. Fei, Y. Xiang, K. Cai, Y. Zhao and Z. Luo, *Adv. Funct. Mater.*, 2020, **30**, 2000229.
39 S. O'Meara, N. A. Cullum and E. A. Nelson, *Cochrane Database Syst. Rev.*, 2009, **1**, CD000265.
40 X. Yang, W. Liu, Y. Shi, G. Xi, M. Wang, B. Liang, Y. Feng, X. Ren and C. Shi, *Acta Biomater.*, 2019, **99**, 220–235.
41 J. Lee, H. N. Choi, H. J. Cha and Y. J. Yang, *Biomacromolecules*, 2023, **24**, 1763–1773.
42 R. Shi, Y. Jin, S. Zhao, H. Yuan, J. Shi and H. Zhao, *Biomed. Pharmacother.*, 2022, **153**, 113463.
43 J.-J. Wu, X.-M. Yuan, C. Huang, G.-Y. An, Z.-L. Liao, G.-A. Liu and R.-X. Chen, *Int. Immunopharmacol.*, 2019, **68**, 218–225.
44 D. R. Griffin, M. M. Archang, C.-H. Kuan, W. M. Weaver, J. S. Weinstein, A. C. Feng, A. Ruccia, E. Sideris, V. Ragkousis, J. Koh, M. V. Plikus, D. Di Carlo, T. Segura and P. O. Scumpia, *Nat. Mater.*, 2021, **20**, 560–569.

45 Y. Lu, Y. Wang, J. Wang, L. Liang, J. Li, Y. Yu, J. Zeng, M. He, X. Wei, Z. Liu, P. Shi and J. Li, *Biomater. Sci.*, 2024, **12**, 3745–3764.
46 A. P. Castano, P. Mroz and M. R. Hamblin, *Nat. Rev. Cancer*, 2006, **6**, 535–545.
47 X. Tang, X. Gu, Y. Wang, X. Chen, J. Ling and Y. Yang, *RSC Adv.*, 2020, **10**, 17280–17287.
48 Y. Feng, S. Qin, H. Li, Y. Yang, Y. Zheng, H. Liu, W. Y. Yap, X. Zhou and J. Wen, *Int. J. Nanomed.*, 2023, **18**, 5183–5195.
49 X. Zhao, B. Guo, H. Wu, Y. Liang and P. X. Ma, *Nat. Commun.*, 2018, **9**, 2784.
50 M. Li, Z. Zhang, Y. Liang, J. He and B. Guo, *ACS Appl. Mater. Interfaces*, 2020, **12**, 35856–35872.
51 K.-W. Zhang, S.-Y. Liu, Y. Jia, M.-L. Zou, Y.-Y. Teng, Z.-H. Chen, Y. Li, D. Guo, J.-J. Wu, Z.-D. Yuan and F.-L. Yuan, *Biomed. Pharmacother.*, 2022, **151**, 113143.
52 L. Si, X. Guo, H. Bera, Y. Chen, F. Xiu, P. Liu, C. Zhao, Y. F. Abbasi, X. Tang, V. Fodera, D. Cun and M. Yang, *Asian J. Pharm. Sci.*, 2023, **18**, 100856.
53 L. Si, X. Guo, H. Bera, Y. Chen, F. Xiu, P. Liu, C. Zhao, Y. F. Abbasi, X. Tang, V. Fodera, D. Cun and M. Yang, *Asian J. Pharm. Sci.*, 2023, **18**, 100856.
54 E. J. Brisbois, J. Bayliss, J. Wu, T. C. Major, C. Xi, S. C. Wang, R. H. Bartlett, H. Handa and M. E. Meyerhoff, *Acta Biomater.*, 2014, **10**, 4136–4142.
55 H. Ren, Z. Zhang, K. Lu, Y. Shen, C. He and X. Chen, *Sci. China: Technol. Sci.*, 2024, **67**, 891–901.
56 K.-E. Toyoshima, K. Asakawa, N. Ishibashi, H. Toki, M. Ogawa, T. Hasegawa, T. Irie, T. Tachikawa, A. Sato, A. Takeda and T. Tsuji, *Nat. Commun.*, 2012, **3**, 784.
57 Y. Kang, L. Xu, J. Dong, X. Yuan, J. Ye, Y. Fan, B. Liu, J. Xie and X. Ji, *Nat. Commun.*, 2024, **15**, 1042.
58 J. Ling, T. Huang, R. Wu, C. Ma, G. Lin, Z. Zhou, J. Wang, Q. Tu, X. Tang, Y. Liu, M. Liu, L. Yang and Y. Yang, *Adv. Funct. Mater.*, 2023, **33**, 202213342.
59 H. Xing, X. Wang, G. Xiao, Z. Zhao, S. Zou, M. Li, J. J. Richardson, B. L. Tardy, L. Xie, S. Komasa, J. Okazaki, Q. Jiang, G. Yang and J. Guo, *Biomaterials*, 2020, **235**, 119784.
60 J. Yu, Y. Shen, J. Luo, J. Jin, P. Li, P. Feng and H. Guan, *Int. Immunopharmacol.*, 2023, **116**, 109680.
61 F. Xu, M. Hu, C. Liu and S. K. Choi, *Biomater. Sci.*, 2017, **5**, 678–685.
62 Y. Yang, J. Zhang, Z. Liu, Q. Lin, X. Liu, C. Bao, Y. Wang and L. Zhu, *Adv. Mater.*, 2016, **28**, 2724.